18th International Conference
ENGINEERING MECHANICS 2012
Svratka, Czech Republic, May 14 – 17, 2012

pp. 1207–1217
Paper #48

BENDING OF FUNCTIONALLY GRADED CIRCULAR PLATES WITH PIEZOELECTRIC LAYER BY THE MLPG METHOD

P. Staňák[*], J. Sladek[*], V. Sladek[*], S. Krahulec[*]

Abstract: *A meshless local Petrov-Galerkin (MLPG) method is applied to solve bending of circular plate with piezoelectric layer attached at the top. Plate is analyzed as a 3D axisymmetric. Functionally graded material properties with continuous variation in the plate thickness direction are considered. Piezoelectric layer with applied nonzero voltage difference acts as a piezoelectric actuator, thus deflection of the plate can be controlled. Local integral equations are defined from the set of governing equations for mechanical and electric fields using appropriate test functions. Spatial variation of all physical fields is approximated by the moving least-squares (MLS) method only in terms of nodes. After performing all spatial integrations the system of ordinary differential equations is finally obtained and solved using Houbolt finite-difference scheme.*

Keywords: ***Meshless local Petrov-Galerkin method (MLPG), moving least-squares (MLS) approximation, piezoelectric actuation, functionally graded materials.***

1. Introduction

Advanced structural systems are required to be low-weight, high-strength and often to have also self-monitoring capabilities. Recent progress in engineering and material sciences offers new possibility in design of such structures; the multifunctional composites (Gibson, 2010) composed of so-called smart materials. Among many smart materials the piezoelectric materials are dominantly used for control and suppression of structural vibration (Adachi et al., 1994) because of their sensory/active capabilities. In the recent years also the functionally graded materials (FGMs) (Suresh and Mortensen, 1998) are widely applied in structural design because of their excellent properties. FGMs are multi-component composite materials in which the volume fraction of the material constituents is varying in a predominant direction. This feature can be used to tune the selected properties into desired value. For example structural element can be designed to have the strength of steel on one side combined with the heat resistance of ceramics on the other side.

Analysis of complex structural systems requires advanced numerical methods because of complex geometry or boundary conditions. Although the well established finite element method (FEM) is applicable to analysis of piezoelectric structures (Benjeddou, 2000), the analysis of materials with continuously nonhomogeneous properties such as FGMs can lead to certain difficulties. The material coefficients in commercial FEM codes are assumed to be constant within an element, thus leading to piecewise homogeneous idealization of FGMs. Boundary element method (BEM) is also not suitable since proper fundamental solution is not available. In the last decade, an increasing attention has been devoted to meshfree or meshless methods for numerical analyses. The motivation is clear from their name; to avoid difficulties associated with mesh of finite elements such as expensive mesh generation, shear locking or above mentioned difficulties in modeling of continuously nonhomogeneous media. The meshless local Petrov-Galerkin (MLPG) method (Atluri, 2004) is considered as a basis for many meshless techniquess. Meshless formulations based on the MLPG were recently applied to laminated plates (Sladek et al, 2010a) and also to piezoelectric plates (Sladek et al, 2010b). Analysis of FGM materials using MLPG was presented in (Sladek et al. 2005, Sladek et al. 2008).

In the present paper the analysis of functionally graded circular plate with homogeneous piezoelectric actuator is presented. Similar problem was analyzed by Tauchert and Ashida (1999)

[*] Ing. Peter Staňák, Prof. Ing. Ján Sládek, DrSc., Prof. RNDr. Vladimír Sládek, DrSc. and Ing. Slavomír Krahulec : Institute of Construction and Architecture, Slovak Academy of Sciences, Dúbravská cesta 9, 845 03, Bratislava; SK, e-mails: peter.stanak@savba.sk, jan.sladek@savba.sk, vladimir.sladek@savba.sk, slavomir.krahulec@savba.sk

using potential function method, although they considered only homogeneous material properties. Fig. 1a) shows proposed geometry with FGM layer labeled by index 1 and piezoelectric layer by index 2. A circular plate together with piezoelectric actuator can be considered as a 3-D axisymmetric body with axis of symmetry passing through the center of the plate. With use of cylindrical coordinates the original 3-D axisymmetric problem can be reduced to 2-D problem considered on the cross-section of the plate (see Fig. 1b). An exponential variation of material properties is assumed for the FGM plate. The coupled electro-mechanical fields are described by constitutive relations and governing partial differential equations (PDEs). Nodal points are spread on the analyzed domain without any restrictions. Small local circular subdomain is introduced around each nodal point. Local integral equations (LIEs) constructed from governing PDEs are defined over these circular subdomains. For a simple shape of subdomains- like circles used here, numerical integration of LIEs can be easily carried out. Moving Least-Squares (MLS) approximation scheme (Lancaster & Salkauskas, 1981) is used to approximate the spatial variations of electric and mechanical fields. MLS scheme ensures C^1 continuity in each layer, but not across the material interface of plate and piezoelectric actuator. Thus MLS approximation is carried out separately in each considered layer. Additional coupling equations are considered for nodes on the interface to ensure the continuity of primary variables, normal components of electric displacements (surface charges) and the equilibrium of the tractions. The essential boundary conditions are satisfied by the collocation of MLS approximation expressions for unknowns at boundary nodes. After performing the MLS approximation a system of ordinary differential equations (ODEs) for certain nodal unknowns is obtained. Houbolt finite difference scheme (Houbolt, 1950) is finally used to solve the system of ODEs.

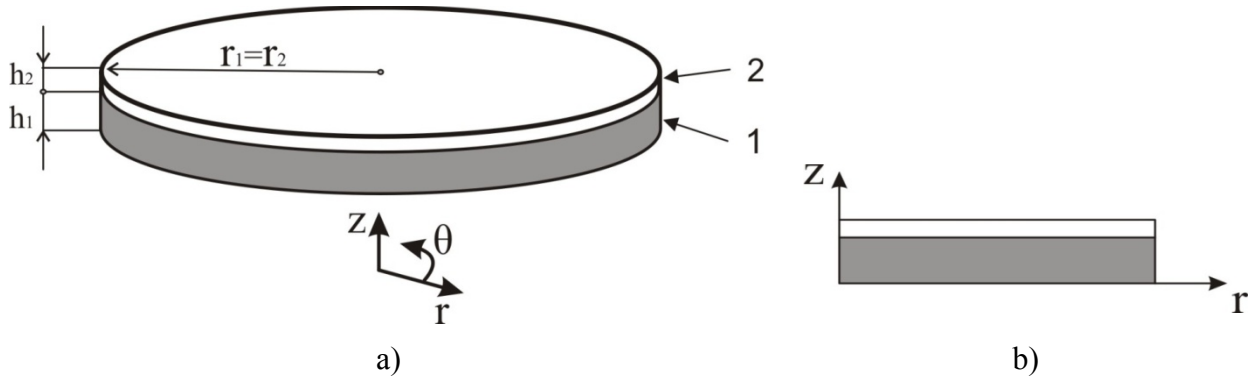

Fig. 1: Geometry of the circular plate: a) original 3-D problem, b) assumed 2-D geometry

2. Local integral equations

Governing equations for general piezoelectric body under quasi-electrostatic assumption is given by the equation of motion for displacements and the first Maxwell's equation for the vector of electric displacements as

$$\sigma_{ij,j}(\mathbf{x},t)+X_i(\mathbf{x},t)=\rho(\mathbf{x})\ddot{u}_i(\mathbf{x},t) \tag{1}$$

$$D_{i,i}(\mathbf{x},t)-R(\mathbf{x},t)=0 \tag{2}$$

where $t, u_i, \sigma_{ij}, D_i, X_i, R, \rho$ are time, displacements, stresses, electric displacements, vector of body forces, volume density of free charges and material density, respectively. The dots over quantity indicate the time derivative. Omitting the acceleration term in Eq. (1) one can easily transform the dynamic problem to static one. The piezoelectric constitutive equations, representing the coupling of mechanical and electric fields, are given by

$$\sigma_{ij}(\mathbf{x},t)=C_{ijkl}\varepsilon_{kl}(\mathbf{x},t)-e_{kij}E_k(\mathbf{x},t) \tag{3}$$

$$D_i(\mathbf{x},t)=e_{ikl}\varepsilon_{kl}(\mathbf{x},t)+h_{ik}E_k(\mathbf{x},t) \tag{4}$$

where C_{ijkl}, e_{kij}, h_{ik} represents elastic, piezoelectric and dielectric material constants, respectively. The strain tensor ε_{ij} and electric field vector E_k are related to mechanical displacements u_i and electric potential ψ by

$$\varepsilon_{ij} = \frac{1}{2}\left(u_{i,j} + u_{j,i}\right) \tag{5}$$

$$E_k = -\psi_{,k} = -\frac{\partial \psi}{\partial x_k} \tag{6}$$

The following essential and natural boundary conditions are assumed for the mechanical field

$$u_i\left(\mathbf{x},t\right) = \tilde{u}_i\left(\mathbf{x},t\right) \text{ on } \Gamma_u,\ \sigma_{ij}n_j = \tilde{T}_i\left(\mathbf{x},t\right) \text{ on } \Gamma_t, \tag{7}$$

and for the electrical field

$$\psi\left(\mathbf{x},t\right) = \tilde{\psi}\left(\mathbf{x},t\right) \text{ on } \Gamma_p,\ D_i n_i = \tilde{Q}\left(\mathbf{x},t\right) \text{ on } \Gamma_q \tag{8}$$

where Γ_u, Γ_t, Γ_p, Γ_q are parts of the global boundary Γ with prescribed displacements, tractions, electric potential and surface density of electric field flux (surface charge density), respectively.

Consider now 2-layer circular plate as shown in Fig. 1a. Base layer, with index 1, has radius r_1 and height h_1, top layer, with index 2 and considered as piezoelectric, has the height h_2 but the same radius $r_2 = r_1$. Owing to the plate geometry, it is convenient to use polar (cylindrical) coordinates $\mathbf{x} = (r,\theta,z)$.

Coupled equations of piezoelectricity can be used for both layers, even if one is not made of piezoelectric material. This is done simply by decoupling the equations using all piezoelectric constants e_{ikl}=0, but keeping nonzero dielectric material constants for non-piezoelectric (base) material.

Since the problem is assumed to be axisymmetric, it can be reduced to 2-D, if cylindrical coordinates are used, as in Fig. 1.b. Thus all physical quantities are independent on angular coordinate θ. Then, for the axisymmetric piezoelectric body we can write the governing equations (1), (2) in the following form

$$\sigma_{rr,r}\left(r,z,t\right) + \sigma_{rz,z}\left(r,z,t\right) + \frac{\sigma_{rr}\left(r,z,t\right) - \sigma_{\theta\theta}\left(r,z,t\right)}{r} + X_r\left(r,z,t\right) = \rho\ddot{u}_r\left(r,z,t\right) \tag{9}$$

$$\sigma_{rz,r}\left(r,z,t\right) + \sigma_{zz,z}\left(r,z,t\right) + \frac{\sigma_{rz}\left(r,z,t\right)}{r} + X_z\left(r,z,t\right) = \rho\ddot{u}_z\left(r,z,t\right) \tag{10}$$

$$D_{r,r}\left(r,z,t\right) + D_{z,z}\left(r,z,t\right) + \frac{D_r\left(r,z,t\right)}{r} = 0 \tag{11}$$

Constitutive equation for mechanical fields (3) is then also rewritten into

$$\sigma_{rr} = c_{11}\varepsilon_{rr} + c_{12}\varepsilon_{\theta\theta} + c_{13}\varepsilon_{zz} - e_{31}E_z \tag{12}$$

$$\sigma_{\theta\theta} = c_{12}\varepsilon_{rr} + c_{11}\varepsilon_{\theta\theta} + c_{13}\varepsilon_{zz} - e_{31}E_z \tag{13}$$

$$\sigma_{zz} = c_{13}\varepsilon_{rr} + c_{13}\varepsilon_{\theta\theta} + c_{33}\varepsilon_{zz} - e_{33}E_z \tag{14}$$

$$\sigma_{rz} = c_{44}\varepsilon_{rz} - e_{15}E_r \tag{15}$$

with mechanical strains specified to be

$$\varepsilon_{rr} = u_{r,r}, \quad \varepsilon_{\theta\theta} = \frac{1}{r}u_r, \quad \varepsilon_{zz} = u_{z,z}, \quad \varepsilon_{rz} = u_{r,z} + u_{z,r} \tag{16}$$

Finally, the constitutive relations for the electric fields are

$$D_r = e_{15}\varepsilon_{rz} + h_{11}E_r \tag{17}$$

$$D_z = e_{31}\varepsilon_{rr} + e_{31}\varepsilon_{\theta\theta} + e_{33}\varepsilon_{zz} + h_{33}E_z \tag{18}$$

The MLPG method is based on the local weak form of the governing equations (9-11) that is written over local subdomain Ω_s. Local subdomain is a small region taken for each node inside the global domain (Atluri, 2004). The local subdomains could be of any geometrical shape; in this paper they posses circular shape just for simplicity. Local weak forms can be written as

$$\begin{aligned}\int_{\Omega_s} \sigma_{rr,r}(r,z,t)\, p^* d\Omega + \int_{\Omega_s} \sigma_{rz,z}(r,z,t)\, p^* d\Omega + \int_{\Omega_s} \frac{1}{r}\left[\sigma_{rr}(r,z,t) - \sigma_{\theta\theta}(r,z,t)\right] p^* d\Omega + \\ + \int_{\Omega_s} X_r(r,z,t)\, p^* d\Omega = \int_{\Omega_s} \rho \ddot{u}_r(r,z,t)\, p^* d\Omega\end{aligned} \tag{19}$$

$$\begin{aligned}\int_{\Omega_s} \sigma_{rz,r}(r,z,t) q^* d\Omega + \int_{\Omega_s} \sigma_{zz,z}(r,z,t) q^* d\Omega + \int_{\Omega_s} \frac{1}{r}\sigma_{rz}(r,z,t) q^* d\Omega + \int_{\Omega_s} X_z(r,z,t) q^* d\Omega = \\ = \int_{\Omega_s} \rho \ddot{u}_z(r,z,t) q^* d\Omega\end{aligned} \tag{20}$$

$$\int_{\Omega_s} D_{r,r}(r,z,t) w^* d\Omega + \int_{\Omega_s} D_{z,z}(r,z,t) w^* d\Omega + \int_{\Omega_s} \frac{1}{r} D_r(r,z,t) w^* d\Omega = 0 \tag{21}$$

where $p^*(\mathbf{x})$, $q^*(\mathbf{x})$, $w^*(\mathbf{x})$ are the test functions.

Local weak forms (19-21) are then the starting point for deriving local integral equations with the use of Gauss divergence theorem and appropriate test functions. Heaviside unit step functions are chosen as test functions for the presented problem in the same way as in (Sladek et al., 2010a). Local integral equations take the form:

$$\begin{aligned}\int_{\partial\Omega_s} \sigma_{rr}(r,z,t) n_r d\Gamma + \int_{\partial\Omega_s} \sigma_{rz}(r,z,t) n_z d\Gamma + \int_{\Omega_s} \frac{1}{r}\left[\sigma_{rr}(r,z,t) - \sigma_{\theta\theta}(r,z,t)\right] d\Omega + \\ + \int_{\Omega_s} X_r(r,z,t)\, d\Omega = \int_{\Omega_s} \rho \ddot{u}_r(r,z,t)\, d\Omega\end{aligned} \tag{22}$$

$$\begin{aligned}\int_{\partial\Omega_s} \sigma_{rz}(r,z,t) n_r d\Gamma + \int_{\partial\Omega_s} \sigma_{zz}(r,z,t) n_z d\Gamma + \int_{\Omega_s} \frac{1}{r}\sigma_{rz}(r,z,t)\, d\Omega + \int_{\Omega_s} X_z(r,z,t)\, d\Omega = \\ = \int_{\Omega_s} \rho \ddot{u}_z(r,z,t)\, d\Omega\end{aligned} \tag{23}$$

$$\int_{\partial\Omega_s} D_r(r,z,t) n_r d\Gamma + \int_{\partial\Omega_s} D_z(r,z,t) n_z d\Gamma + \int_{\Omega_s} \frac{1}{r} D_r(r,z,t)\, d\Omega = 0 \tag{24}$$

where $\partial\Omega_s$ represents boundary of the local subdomain Ω_s and n_i is the unit outward normal vector.

A meshless approximation is convenient for numerical solution of local integral equations. The Moving least-squares (MLS) approximation can be used for the approximation of displacement and electric potential fields $u_r(\mathbf{x},t)$, $u_z(\mathbf{x},t)$, $\psi(\mathbf{x},t)$ by $u_r^h(\mathbf{x},t)$, $u_z^h(\mathbf{x},t)$, $\psi^h(\mathbf{x},t)$ in terms of nodal values as

$$u_r(\mathbf{x},t) \cong u_r^h(\mathbf{x},t) = \sum_{i=1}^{n} \phi^i(\mathbf{x}) \hat{u}_r^i(t) \tag{25}$$

$$u_z(\mathbf{x},t) \cong u_z^h(\mathbf{x},t) = \sum_{i=1}^{n} \phi^i(\mathbf{x}) \hat{u}_z^i(t) \tag{26}$$

$$\psi(\mathbf{x},t) \cong \psi^h(\mathbf{x},t) = \sum_{i=1}^{n} \phi^i(\mathbf{x}) \hat{\psi}^i(t) \tag{27}$$

where the nodal values $\hat{u}_r^i(t)$, $\hat{u}_z^i(t)$, $\hat{\psi}^i(t)$ are so called fictitious parameters for the displacements and electric potential, and $\phi^i(\mathbf{x})$ is called the MLS shape function defined over *n* nodes located in a support domain of MLS approximation. However, MLS support domain must contain only nodes from a single layer bounded by the two-material interface due to discontinuities of strains and electric vector on the interface of the plate and actuator (Sladek et al, 2009). The appropriate derivatives can be obtained with use of the shape function derivative as shown in (Atluri, 2004). Derivatives of displacements and electric potential are then given as

$$u_{k,l}^h(\mathbf{x},t) = \sum_{i=1}^{n} \phi_{,l}^i(\mathbf{x}) \hat{u}_k^i(t) \quad , \quad \psi_{,l}^h(\mathbf{x},t) = \sum_{i=1}^{n} \phi_{,l}^i(\mathbf{x}) \hat{\psi}^i(t) \tag{28}$$

with indices $k,l = (r,z)$.

C^1 continuity of the MLS approximation in each domain (layer) is ensured by the fourth-order spline type weight function used for the construction of the shape function $\phi^i(\mathbf{x})$ (Atluri, 2004).

Applying Eqs. (25-27) for approximation of trial functions $u_r(\mathbf{x},t)$, $u_z(\mathbf{x},t)$, $\psi(\mathbf{x},t)$ and their derivatives in constitutive relations (12-18) and their insertion into local integral equations (22-24) is leading to discretized local integral equations in the following form

$$\begin{aligned}
&\sum_{i=1}^{n} \hat{u}_r^i(t) \int_{\partial\Omega_s} \left[c_{11} n_r(\mathbf{x}) \phi_{,r}^i(\mathbf{x}) + \frac{c_{12}}{r} n_r(\mathbf{x}) \phi^i(\mathbf{x}) + c_{44} n_z(\mathbf{x}) \phi_{,z}^i(\mathbf{x}) \right] d\Gamma + \\
&+ \sum_{i=1}^{n} \hat{u}_r^i(t) \int_{\Omega_s} \left[\frac{c_{11}}{r} \phi_{,r}^i(\mathbf{x}) + \frac{c_{12}}{r^2} \phi^i(\mathbf{x}) - \frac{c_{11}}{r^2} \phi^i(\mathbf{x}) - \frac{c_{12}}{r} \phi_{,r}^i(\mathbf{x}) \right] d\Omega - \\
&- \sum_{i=1}^{n} \hat{\ddot{u}}_r^i(t) \int_{\Omega_s} \rho \phi^i(\mathbf{x}) d\Omega + \sum_{i=1}^{n} \hat{u}_z^i(t) \int_{\partial\Omega_s} \left[c_{13} n_r(\mathbf{x}) \phi_{,z}^i(\mathbf{x}) + c_{44} n_z(\mathbf{x}) \phi_{,r}^i(\mathbf{x}) \right] d\Gamma + \\
&+ \sum_{i=1}^{n} \hat{\psi}^i(t) \int_{\partial\Omega_s} \left[e_{31} n_r(\mathbf{x}) \phi_{,z}^i(\mathbf{x}) + e_{15} n_z(\mathbf{x}) \phi_{,r}^i(\mathbf{x}) \right] d\Gamma = -\int_{\Omega_s} X_r(r,z,t) d\Omega
\end{aligned} \tag{29}$$

$$\sum_{i=1}^{n}\hat{u}_r^i(t)\int_{\partial\Omega_s}\left[c_{44}n_r(\mathbf{x})\phi_{,z}^i(\mathbf{x})+\frac{c_{13}}{r}n_z(\mathbf{x})\phi^i(\mathbf{x})+c_{13}n_z(\mathbf{x})\phi_{,r}^i(\mathbf{x})\right]d\Gamma+$$
$$+\sum_{i=1}^{n}\hat{u}_r^i(t)\int_{\Omega_s}\frac{c_{44}}{r}\phi_{,z}^i(\mathbf{x})d\Omega+\sum_{i=1}^{n}\hat{u}_z^i(t)\int_{\partial\Omega_s}\left[c_{33}n_z(\mathbf{x})\phi_{,z}^i(\mathbf{x})+c_{44}n_r(\mathbf{x})\phi_{,r}^i(\mathbf{x})\right]d\Gamma+$$
$$+\sum_{i=1}^{n}\hat{u}_z^i(t)\int_{\Omega_s}\frac{c_{44}}{r}\phi_{,r}^i(\mathbf{x})d\Omega-\sum_{i=1}^{n}\hat{\ddot{u}}_z^i(t)\int_{\Omega_s}\rho\phi^i(\mathbf{x})d\Omega+ \tag{30}$$
$$+\sum_{i=1}^{n}\hat{\psi}^i(t)\int_{\partial\Omega_s}\left[e_{15}n_r(\mathbf{x})\phi_{,r}^i(\mathbf{x})+e_{33}n_z(\mathbf{x})\phi_{,z}^i(\mathbf{x})\right]d\Gamma+\sum_{i=1}^{n}\hat{\psi}^i(t)\int_{\Omega_s}\frac{e_{15}}{r}\phi_{,r}^i(\mathbf{x})d\Omega=$$
$$=-\int_{\Omega_s}X_z(r,z,t)d\Omega$$

$$\sum_{i=1}^{n}\hat{u}_r^i(t)\int_{\partial\Omega_s}\left[e_{15}n_r(\mathbf{x})\phi_{,z}^i(\mathbf{x})+\frac{e_{31}}{r}n_z(\mathbf{x})\phi^i(\mathbf{x})+e_{31}n_z(\mathbf{x})\phi_{,r}^i(\mathbf{x})\right]d\Gamma+$$
$$+\sum_{i=1}^{n}\hat{u}_r^i(t)\int_{\Omega_s}\frac{e_{15}}{r}\phi_{,z}^i(\mathbf{x})d\Omega+\sum_{i=1}^{n}\hat{u}_z^i(t)\int_{\partial\Omega_s}\left[e_{15}n_r(\mathbf{x})\phi_{,r}^i(\mathbf{x})+e_{33}n_z(\mathbf{x})\phi_{,z}^i(\mathbf{x})\right]d\Gamma+$$
$$+\sum_{i=1}^{n}\hat{u}_z^i(t)\int_{\Omega_s}\frac{e_{15}}{r}\phi_{,r}^i(\mathbf{x})d\Omega-\sum_{i=1}^{n}\hat{\psi}^i(t)\int_{\partial\Omega_s}\left[h_{11}n_r(\mathbf{x})\phi_{,r}^i(\mathbf{x})+h_{33}n_z(\mathbf{x})\phi_{,z}^i(\mathbf{x})\right]d\Gamma- \tag{31}$$
$$-\sum_{i=1}^{n}\hat{\psi}^i(t)\int_{\Omega_s}\frac{h_{11}}{r}\phi_{,r}^i(\mathbf{x})d\Omega=0$$

Collocation approach is used to impose essential boundary conditions directly, using MLS variable approximations (25-27). For natural boundary conditions local integral equations are written for the nodes on the global boundary.

Interface between two layers of the plate represents a discontinuity. The plate must be partitioned to two patches with different material properties for the presented numerical modeling approach. Patches or layers are discretized by meshfree nodes individually. Double nodes are defined on the interface. One node belongs to each layer. Except the condition of coincidence of interface nodes there is no restriction on the node location in the presented approach. For these interface nodes one has to specify coupling conditions in order to ensure the continuity of displacements, potentials, flux of electric displacements and the equilibrium of the tractions across the interface as

$$^1u_r(\mathbf{x}^l,t)=\,^2u_r(\mathbf{x}^l,t),\quad ^1T_r(\mathbf{x}^l,t)+\,^2T_r(\mathbf{x}^l,t)=0 \tag{32}$$

$$^1u_z(\mathbf{x}^l,t)=\,^2u_z(\mathbf{x}^l,t),\quad ^1T_z(\mathbf{x}^l,t)+\,^2T_z(\mathbf{x}^l,t)=0 \tag{33}$$

$$^1\psi(\mathbf{x}^l,t)=\,^2\psi(\mathbf{x}^l,t),\quad ^1Q(\mathbf{x}^l,t)+\,^2Q(\mathbf{x}^l,t)=0 \tag{34}$$

indices 1, 2 indicate the corresponding layer and $\mathbf{x}^l$ is an interface node.

Collocation approach is again used based on the MLS approximation (7). For example, the equilibrium of radial displacements (first part of Eq. 32) is specified as

$$\sum_{i=1}^{^1n}\phi^i(\mathbf{x}^l)\,^1\hat{u}_r^i=\sum_{j=1}^{^2n}\phi^j(\mathbf{x}^l)\,^2\hat{u}_r^j \tag{35}$$

In the same manner the equilibrium of tractions and electric charge can be specified, based on the second part of Eqs. (7, 8).

Collecting the discretized local integral equations together with the discretized boundary conditions and interface conditions, one obtains a complete system of ordinary differential equations (ODE) which can be rearranged in such a way that all known quantities are on the r.h.s. Thus, in the matrix form the system becomes

$$\mathbf{A}\ddot{\mathbf{x}} + \mathbf{C}\mathbf{x} = \mathbf{Y} \tag{36}$$

This system of ODE can be solved by the Houbolt finite-difference scheme (Houbolt, 1950; Sladek et al., 2010a). In this method "acceleration" term is defined as

$$\ddot{\mathbf{x}}_{t+\Delta t} = \frac{2\mathbf{x}_{t+\Delta t} - 5\mathbf{x}_t + 4\mathbf{x}_{t-\Delta t} - \mathbf{x}_{t-2\Delta t}}{\Delta t^2} \tag{37}$$

where Δt is the time step. The value of the time-step has to be appropriately selected with respect to material parameters (elastic wave velocities).

3. Numerical solution

For the numerical examples functionally graded graphite/epoxy circular plate is considered with radius $r_1 = 0.3\text{m}$ and thickness $h_1 = 0.02\text{m}$. For the top layer of the thickness $h_2 = 0.01\text{m}$ PZT-4 piezoelectric material is considered. The plate is loaded with uniform load of $\sigma_0 = 10000\text{Pa}$ and varying electric potential at the top. Potential at the interface is vanishing. For the approximation of unknown field quantities in FGM layer 847 nodes were used and 726 nodes were specified for the piezoelectric layer. Material properties of the graphite/epoxy layer are graded using exponential variations

$$f_{ij}(\mathbf{x}) = f_{ij0}\exp(\gamma_f z) \tag{38}$$

where the symbol f_{ij} is commonly used for particular material coefficients and f_{ij0} correspond to the material parameters at the bottom surface of the FG layer. It should be noted that various exponential coefficients γ_f can be used for the individual material parameters. In presented analysis two different values of the exponential coefficient $\gamma_f = 34.6575$ and 20.273 are used for each graded material coefficient. For the first coefficient $\gamma_f = 34.6575$ material parameters are doubled with respect to ones at the bottom surface. In other words, such a gradation will gradually increase material coefficients defined at the bottom $(z = 0)$ to twice that large coefficients at the top $(z = h_1)$ of the graphite/epoxy plate.

The material coefficients of the graphite/epoxy layer are:

$$c_{110} = 10.2\cdot 10^{10}\,Nm^{-2}\ ,\ c_{120} = 4.98\cdot 10^{10}\,Nm^{-2}\ ,\ c_{130} = c_{230} = 6.86\cdot 10^{9}\,Nm^{-2}\ ,$$
$$c_{330} = 1.09\cdot 10^{10}\,Nm^{-2}\ ,\ c_{440} = 2.87\cdot 10^{9}\,Nm^{-2}\ ,\ e_{150} = e_{310} = e_{330} = 0\,Cm^{-2}\ ,$$
$$h_{110} = 3.09\cdot 10^{-11}C(Vm)^{-1}\ ,\quad h_{330} = 2.65\cdot 10^{-11}C(Vm)^{-1}\ ,\ \rho = 1578\,\text{kg/m}^3$$

Piezoelectric PZT-4 layer posses these material properties:

$$c_{11} = 13.9\cdot 10^{10}\,Nm^{-2}\ ,\ c_{12} = 7.78\cdot 10^{10}\,Nm^{-2}\ ,\ c_{13} = c_{23} = 7.43\cdot 10^{10}\,Nm^{-2}\ ,$$
$$c_{33} = 11.5\cdot 10^{10}\,Nm^{-2}\ ,\ c_{44} = 2.56\cdot 10^{10}\,Nm^{-2}\ ,$$
$$e_{15} = 12.7\,Cm^{-2}\ ,\ e_{31} = -5.2\,Cm^{-2}\ ,\quad e_{33} = 15.1\,Cm^{-2}\ ,$$
$$h_{11} = 6.46\cdot 10^{-9}C(Vm)^{-1}\ ,\quad h_{33} = 5.62\cdot 10^{-9}C(Vm)^{-1}\ ,\ \rho = 7500\,\text{kg/m}^3\ .$$

In the first numerical example two different exponential variations are applied. Variation represented by Eq. (38) increases (grades) material properties from bottom to the top, while following variation

$$f_{ij}(\mathbf{x}) = f_{ij0}\left(d - \exp(\gamma_f z)\right) \tag{39}$$

grades material properties in opposite direction. Constant d depends on the coefficients γ_f, values d=3 and d=2.5 are used, respectively. Results are compared to FEM-ANSYS solution with the fine mesh. For FGM material modeling the piecewise homogeneous approach is adopted. Fig. 2 presents variation of deflection for simply supported plate with the radial coordinate under static mechanical loading and vanishing surface charge density. For both gradation schemes the coefficient $\gamma_f = 34.6575$. One can clearly observe that material gradation according to Eq. (39) gives lower deflection compared to Eq. (38). This must hold true since increase of material constants in direction towards the plate center has smaller effect on flexural stiffness compared to increase of material parameters out of the center, as in case of Eq. (39). Thus exponential variation (39) should be preferred in cases of 2-layer plates.

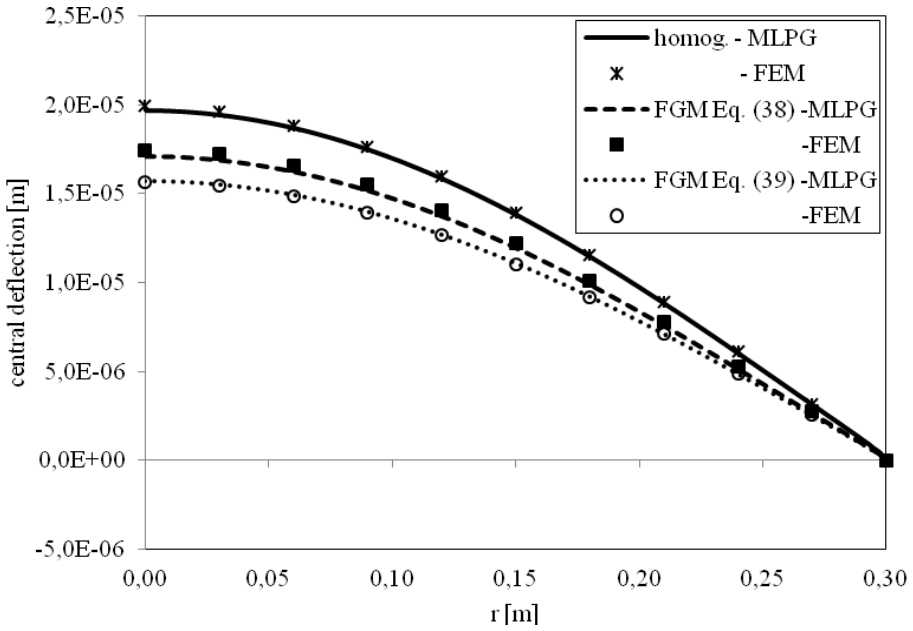

Fig. 2: Variation of central deflection with radial coordinate for simply supported plate with different material gradations

In the Fig. 3 the effect of exponential coefficient γ_f is observed. Pure mechanical load is applied again. Exponential variation (39) is assumed. One can observe that deflection of the plate with $\gamma_f = 20.273$ is very close to one obtained for variation (38) as shown in Fig. 2. Very good agreement between MLPG and FEM results can be observed. Effect of deflection suppression by active piezoelectric layer is well observed in Fig. 4. FGM exponential coefficient $\gamma_f = 34.6575$ is used. It is clearly observable that for FGM plate the deflection is almost totally suppressed. If electric potential is not specified, vanishing values of normal components of electric displacement must be specified.

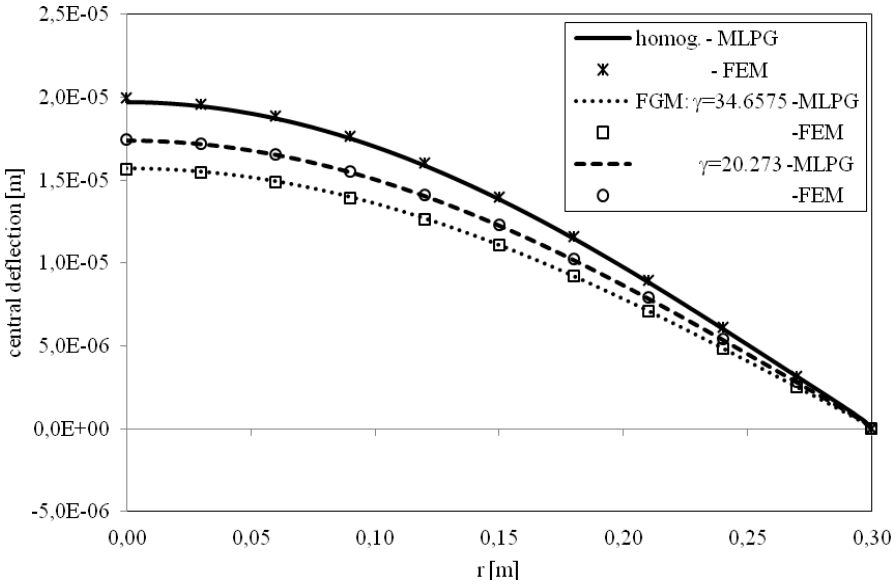

Fig. 3: Variation of central deflection with radial coordinate for simply supported plate with two different exponential coefficients

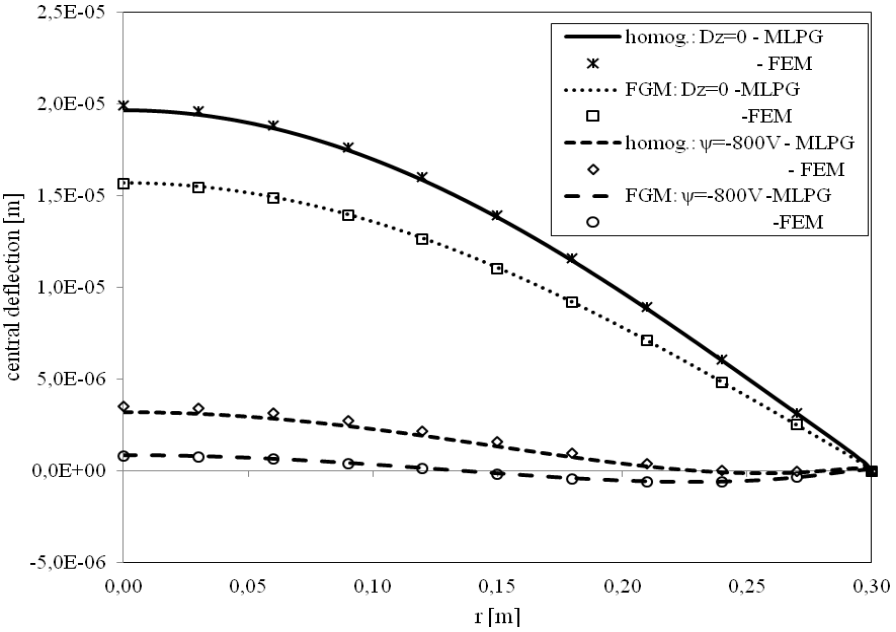

Fig. 4: Variation of central deflection with radial coordinate for simply supported plate under mechanical and electric load

Clamped circular plates are also analyzed. Both electric and mechanical loads are assumed. FGM exponential coefficient $\gamma_f = 34.6575$ is used again. Fig. 5 shows variation of deflection for clamped plates with homogeneous and FGM graphite/epoxy layer. Potential load $\psi = -800\,\mathrm{V}$ is not sufficient to suppress the deflection completely as in case of simply supported plate, larger values have to be applied. Note that negative potential difference must be applied between the surfaces of piezoelectric layer. Positive values would act in opposite sense, thus increasing the deflection.

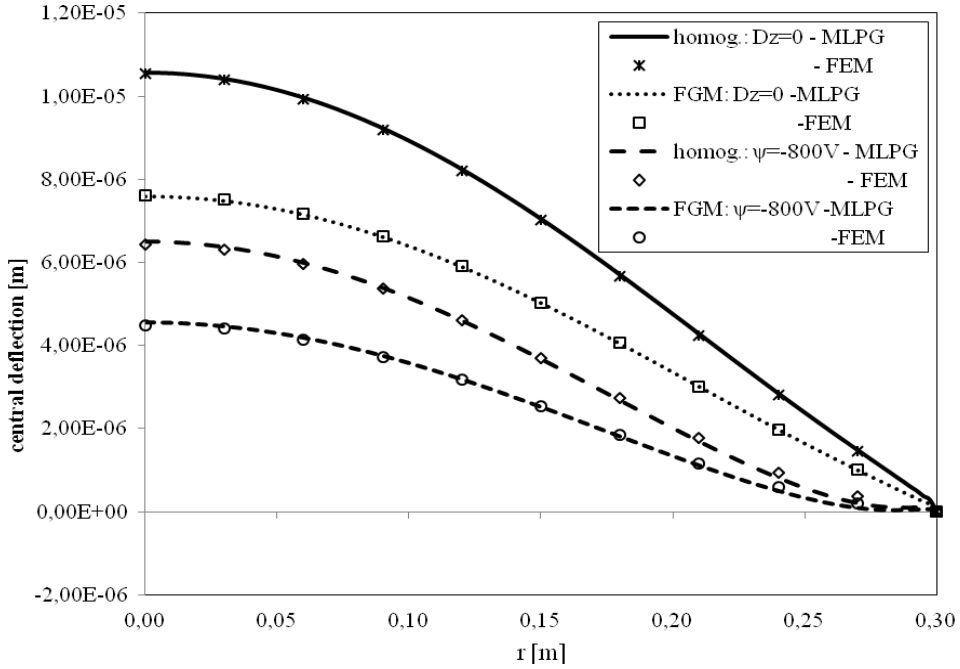

Fig. 5: Variation of central deflection with radial coordinate for clamped plate under mechanical and electric load

Response of simply supported 2-layer plate is also investigated under an impact mechanical load with Heaviside time variation. Numerical calculations are carried out for 100 time steps and a time-step size $\Delta\tau = 0.3\times10^{-4}\,s$. The time variation of the deflection at the plate center $\left(r=0; z=h_1/2\right)$ is given in Fig. 6. The value of the central deflection of the FGM plate is smaller than that of the homogeneous plate. It is due to the higher stiffness of the FGM plate. The peak deflection is shifted to shorter time instants for the FGM plate, where the flexural rigidity is higher and the mass density is the same for the FGM and homogeneous plates. Then, the wave velocities of the FGM plate are larger.

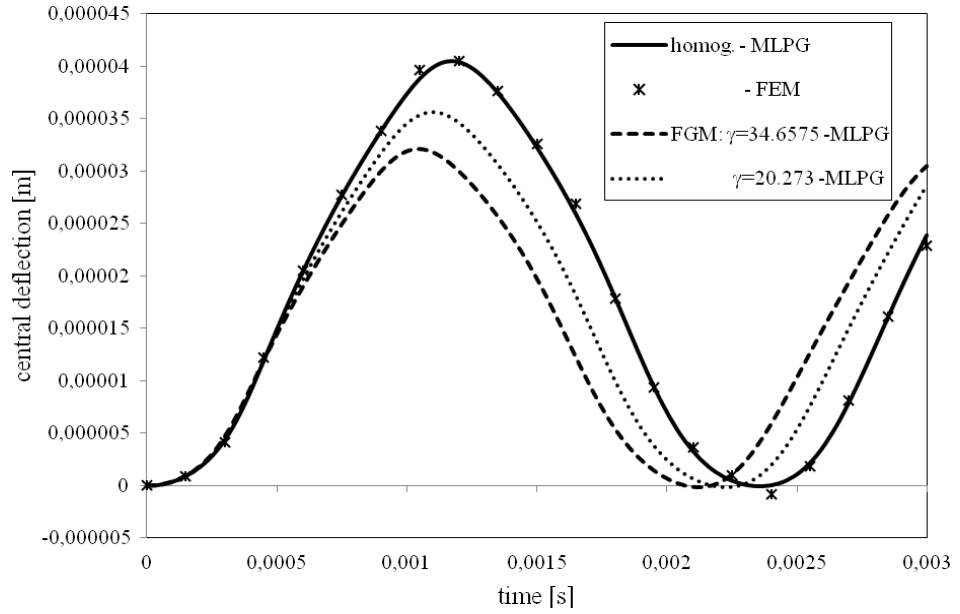

Fig. 6: Time variation of the central deflection for a simply supported plate under an impact mechanical load

4. Conclusion

A meshless local Petrov-Galerkin (MLPG) method was presented for the modeling and analysis of plate bending of 2-layer circular plate with functionally graded bottom layer and active piezoelectric layer. Special treatment of material interface was employed through coupling of interface variables. The MLS approximation was adopted for approximation of unknown physical quantities in each layer separately. Proposed method is a truly meshless method as no elements were used for approximation or for integration of unknowns. Numerical examples showed the effect of material grading and active piezoelectric layer on enhancement of the plate's flexural strength.

Acknowledgement

The authors gratefully acknowledge the support by the Slovak Science and Technology Assistance Agency registered under number APVV-0014-10.

References

Adachi, A., Kitamura, Y., Iwatsubo, T. (2004) Integrated design of piezoelectric damping system for flexible structure. *Applied Acoustics*, 65, pp. 293-310.

Atluri, S. N. (2004) *The meshless method (MLPG) for domain & BIE discretizations*. Tech Science Press, Forsyth, USA.

Benjeddou, A. (2000) Advances in piezoelectric finite element modeling of adaptive structural elements: a survey. *Computers and Structures*, 76, pp. 347-363.

Gibson, R. F. (2010) A review of recent research on mechanics of multifunctional composite materials and structures. *Composite structures*, 92, pp. 2793-2810.

Houbolt, J. C. (1950) A recurrence matrix solution for the dynamic response of elastic aircraft. *Journal of Aeronautical Sciences,* 17, pp. 371-376.

Lancaster, P., Salkauskas, T. (1981) Surfaces generatad by moving least-square methods. *Math. Comput*., 37, pp. 141-158.

Sladek, J., Sladek, V., Stanak, P., Zhang, Ch. (2010a) Meshless Local Petrov-Galerkin (MLPG) Method for Laminate Plates under Dynamic Loading. *CMC- Computers, Materials & Continua*, 15, pp. 1-26.

Sladek, J., Sladek, V., Stanak, P., Pan, E. (2010b) The MLPG for bending of electroelastic plates. *CMES- Computer Modeling in Engineering & Sciences*, 64, pp. 267-298.

Sladek, J., Sladek, V., Solek, P. & Saez, A. (2008) Dynamic 3D axisymmetric problems in continuously nonhomogeneous piezoelectric solids. *International Journal of Solids and Structures*, 45, pp. 4523-4542.

Sladek, J., Sladek, V., Wunsche, M. & Zhang , C. (2009) Interface crack problems in anisotropic solids analyzed by the MLPG. *CMES - Computer Modeling in Engineering & Sciences,* 54, pp. 223-252.

Sladek, V., Sladek, J. & Tanaka, M. (2005) Local Integral Equations and two Meshless Polynomial Interpolations with Application to Potential Problems in Non-homogeneous Media. *CMES- Computer Modeling in Engineering & Sciences*, 7, pp. 69-83.

Suresh, S., Mortensen, A. (1998) *Fundamentals of Functionally Graded Materials*. Institute of Materials, London

Tauchert, T. R., Ashida, F. (1999) Application of the potential function method in piezothermoelasticity: Solutions for composite circular plates. *Journal of Thermal Stresses*, 22, pp. 387-420.